Deep Learning-based Interference Mitigation of SF-Modulated Signals for FMCW Systems

Yeong Choi, Chanul Park, and Seongwook Lee
Department of Electrical and Electronics Engineering
College of ICT Engineering, Chung-Ang University
Seoul, Republic of Korea
{dodrmfl02, qkrcksdnf97, seongwooklee}@cau.ac.kr

***Abstract*—We present a method for mitigating interference in frequency-modulated continuous-wave (FMCW) systems caused by stepped-frequency FMCW (SF-FMCW) signals. Mutual interference between radar systems can lead to a raised noise floor and obscured targets, resulting in degraded target detection performance. While conventional FMCW-to-FMCW interference is well-documented, the emergence of varied radar waveforms, such as SF-FMCW, introduces new challenges. Because these characteristics are different from those of typical FMCW-to-FMCW interference, a novel mitigation method is required. To address this issue, we propose a deep learning-based method to mitigate SF-FMCW-induced interference in FMCW systems. The proposed SF-FMCW interference mitigation network (SF-IMNet) is designed to predict the two-dimensional interference component. Then, by subtracting this predicted interference from the received signal, it is possible to eliminate the interference while minimizing the loss of critical target information. Simulation results show that the proposed method achieves a signal-to-interference-plus-noise ratio (SINR) of 22.94 dB and a correlation coefficient of 0.997 under an input SINR of −10 dB. In addition, the method provides consistent performance in both equal-bandwidth and different-bandwidth interference scenarios. Compared with existing methods, the proposed SF-IMNet improves the SINR by up to 24.1 dB.**

***Index Terms*—deep learning, interference mitigation, stepped-frequency frequency-modulated continuous-wave (SF-FMCW).**

I. Introduction

The rapid development of autonomous driving has increased the need for reliable sensing [1]–[3]. Radar systems, particularly frequency-modulated continuous-wave (FMCW) radars, are widely adopted due to their reliability in harsh conditions and cost-effectiveness [4]–[6]. However, as radar-equipped vehicles become more common, mutual interference has emerged as a major concern [7]. This interference elevates the noise floor and introduces ghost targets, which can severely degrade target detection performance [8].

To overcome these interference challenges while maintaining the hardware advantages of conventional FMCW systems, stepped-frequency FMCW (SF-FMCW) has recently emerged as a promising waveform [9]. By shifting the center frequency of each chirp in a stepwise manner, SF-FMCW systems can reduce mutual interference while achieving high-resolution sensing [10], [11]. However, this introduces severe challenges in heterogeneous environments. When SF-FMCW signals are received by a conventional FMCW system, the mismatch between their waveform structures leads to interference patterns that are different from typical target-reflected FMCW signals. These patterns can obscure weak target-reflected signals. Although several interference mitigation techniques, such as amplitude-based suppression [12] and time–frequency domain interpolation [13], have been explored for FMCW systems, their performance significantly degrades when faced with SF-FMCW interference.

To address these limitations, we propose the SF-FMCW interference mitigation network (SF-IMNet), a deep learning framework that estimates the interference component and mitigates its effect on target-reflected FMCW signals. Unlike conventional suppression-based methods that discard interference-contaminated signals, SF-IMNet predicts a two-dimensional interference map using a U-Net architecture and subtracts it from the received signal. By reconstructing and removing only the interference term, the proposed method can preserve the target-reflected signal and prevent the loss of target information.

The main contributions of this paper are summarized as follows:

- We formulate a signal model for SF-FMCW interference and analyze the resulting signal distortions in both the time domain and the frequency domain.
- We propose SF-IMNet, a deep learning-based framework for the mitigation of SF-FMCW interference. The network estimates the interference components within the input signal. Then, by removing these components from the original received signal, we can effectively restore the signal to its interference-free state.
- We validate the proposed method through simulations and compare it with conventional interference mitigation methods.

The remainder of this paper is organized as follows. In Section II, we formulate the signal model of an FMCW system under SF-FMCW interference and analyze the resulting distortion patterns. Next, we introduce the proposed deep learning-based interference mitigation framework in Section III. Then, in Section IV, we describe the simulation setup and evaluate the performance of the proposed method. Finally, we conclude this paper in Section V.

II. SF-FMCW-to-FMCW Interference Analysis

The FMCW system transmits a linear frequency-modulated chirp, and the transmit signal is expressed as

$$s_{\mathrm{F}}(t) = A_{\mathrm{F}} \exp\left(j2\pi\left(f_c t + \frac{B_{\mathrm{F}}}{2T}t^2\right)\right), \ (p-1)T \le t \le pT, \tag{1}$$

where A_{F}, f_c, B_{F}, T, and p denote the transmit amplitude, carrier frequency, bandwidth, chirp duration, and chirp index, respectively. The SF-FMCW signal is also based on linear frequency modulation, and it applies a stepwise increment to the carrier frequency of each successive chirp. The transmit signal of the SF-FMCW system can be expressed as

$$s_{\mathrm{SF}}(t) = A_{\mathrm{SF}} \exp\left(j2\pi\left(\left(f_c' + (p-1)\Delta f\right)t + \frac{B_{\mathrm{SF}}}{2T}t^2\right)\right), \quad (p-1)T \le t \le pT, \tag{2}$$

where A_{SF}, f_c', Δf, and B_{SF} denote the signal amplitude, carrier frequency, frequency step size between chirps, and chirp bandwidth of the SF-FMCW signal, respectively. The scenario in Fig. 1 shows an FMCW system that receives signals from L reflecting targets together with an interfering SF-FMCW signal. Both components arrive at the receiver with propagation-dependent attenuation and delay. The received passband signal can be expressed as

$$r(t) = \sum_{l=1}^{L} \sigma_{\mathrm{F},l}\, s_{\mathrm{F}}(t-\tau_l) + \sigma_{\mathrm{SF}}\, s_{\mathrm{SF}}(t-\tau') + n_{\mathrm{r}}(t), \tag{3}$$

where $\sigma_{\mathrm{F},l}$ is the attenuation factor of the l-th target echo and τ_l is the round-trip delay of the l-th target. In addition, σ_{SF} is the attenuation of the interfering SF-FMCW signal, τ' is an effective timing offset due to propagation delay and timing asynchrony between radars, and $n_{\mathrm{r}}(t)$ is the additive white Gaussian noise (AWGN).

After dechirping, the resulting signal can be expressed as

$$\begin{aligned} y(t) &= r(t)\, s_{\mathrm{F}}^*(t) \\ &= \sum_{l=1}^{L} \sigma_{\mathrm{F},l}\, s_{\mathrm{F}}(t-\tau_l) s_{\mathrm{F}}^*(t) \\ &\quad + \sigma_{\mathrm{SF}}\, s_{\mathrm{SF}}(t-\tau') s_{\mathrm{F}}^*(t) + n_{\mathrm{r}}(t)\, s_{\mathrm{F}}^*(t) \\ &= x(t) + i(t) + n(t), \end{aligned} \tag{4}$$

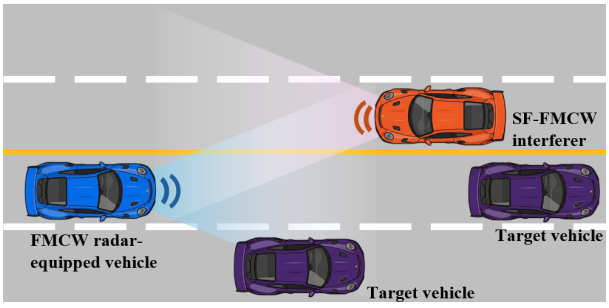

Fig. 1. Interference scenario in a dense automotive environment, where an FMCW radar-equipped vehicle observes multiple targets under SF-FMCW interference.

where $x(t)$, $i(t)$, and $n(t)$ denote the target-reflected FMCW signal, the SF-FMCW interference component after dechirping, and the AWGN after dechirping, respectively.

The dechirped signal $y(t)$ is then passed through a low-pass filter (LPF) and sampled at a rate of T_s. Assuming that the FMCW system and the SF-FMCW system operate at the same carrier frequency, the discretized interference component obtained through sampling can be expressed as

$$\begin{aligned} \mathbf{I}[n,p] \approx \sigma_{\mathrm{SF}} \exp\Bigg(j2\pi\Bigg[&\left(\frac{B_{\mathrm{SF}}}{T}\tau' + \Delta f - (B_{\mathrm{F}} - B_{\mathrm{SF}})\right) nT_s \\ &+ \left(B_{\mathrm{SF}}\tau' + \Delta f\,(T_s + 2T) - (B_{\mathrm{F}} - B_{\mathrm{SF}})(T_s + T)\right) p \\ &+ \left(B_{\mathrm{F}} - B_{\mathrm{SF}} - \Delta f\right) np\, T_s + \frac{B_{\mathrm{F}} - B_{\mathrm{SF}}}{T}\, n^2 T_s^2 \\ &+ \left(\frac{B_{\mathrm{F}} - B_{\mathrm{SF}}}{2} - \Delta f\right) p^2 T\Bigg] + \phi_0\Bigg), \end{aligned} \tag{5}$$

where n denotes the fast-time sample index, p denotes the slow-time sample index, and ϕ_0 denotes a constant phase term.

If the FMCW system and the SF-FMCW interferer share the same chirp bandwidth, (5) can be expressed as

$$\begin{aligned} \mathbf{I}_{\mathrm{eq}}[n,p] \approx \sigma_{\mathrm{SF}} \exp\Bigg(j2\pi\Bigg[&\left(\frac{B_{\mathrm{SF}}}{T}\tau' + \Delta f\right) nT_s \\ &+ \left(B_{\mathrm{SF}}\tau' + \Delta f\,(T_s + 2T)\right) p \\ &- \Delta f np T_s - \Delta f p^2 T\Bigg] + \phi_0\Bigg). \end{aligned} \tag{6}$$

The effects of dechirping and LPF processing on an SF-FMCW signal in an FMCW system are shown in Fig. 2. In Fig. 2 (a), the FMCW system and the SF-FMCW interferer share the same chirp bandwidth. After dechirping, the SF-FMCW interference exhibits a step-like frequency pattern due to the piecewise frequency increments of the SF-FMCW interferer. Signal components whose instantaneous frequencies exceed the LPF cutoff are suppressed by the filtering process.

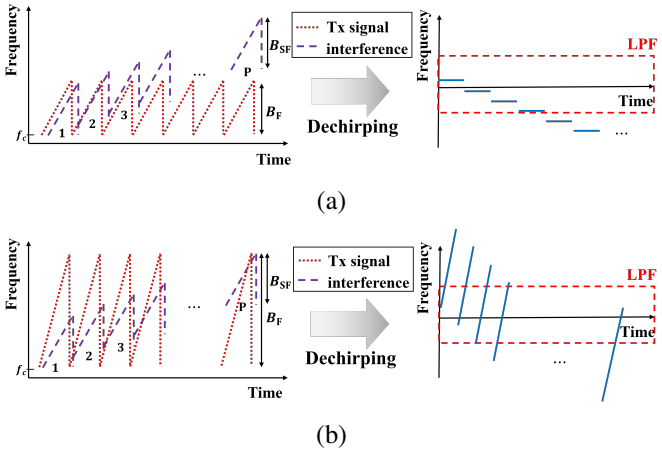

Fig. 2. Dechirped and LPF-processed SF-FMCW interference observed at an FMCW system: (a) the equal-bandwidth case ($B_{\mathrm{SF}} = B_{\mathrm{F}}$) and (b) the different-bandwidth case ($B_{\mathrm{SF}} \neq B_{\mathrm{F}}$).

However, interference components that fall within the LPF passband remain after filtering and continue to affect the received signal. If the FMCW system and the SF-FMCW interferer operate with different chirp bandwidths, a different behavior is observed, as shown in Fig. 2 (b). In this case, the dechirped SF-FMCW interference exhibits a frequency slope within each chirp, which produces a tilted pattern in the time domain. As a result, a portion of the interference remains within the LPF passband and introduces distortion.

The sampled signal is then processed using a two-dimensional fast Fourier transform (FFT) along the fast-time and slow-time dimensions to generate the corresponding range and velocity profiles. The impact of SF-FMCW interference on the time-domain samples and the corresponding range profiles is shown in Fig. 3. In Fig. 3 (a), periodic fluctuations appear in the time-domain signal in the equal-bandwidth case, whereas short, high-amplitude spikes arise in the different-bandwidth case. These distinct temporal characteristics lead to different behaviors in the range profile. In Fig. 3 (b), the equal-bandwidth case produces periodic spectral peaks in the range profile, which are induced by the coupling term $-\Delta f\, T_s\, np$ in (6). In contrast, the transient interference observed in the different-bandwidth case results in wideband spectral leakage across the range dimension, thereby elevating the noise floor. These effects highlight the need for a novel interference mitigation method.

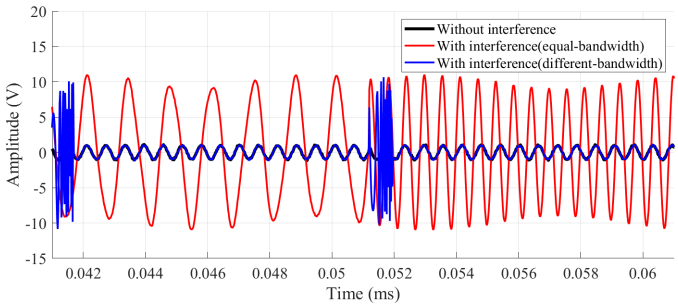

(a)

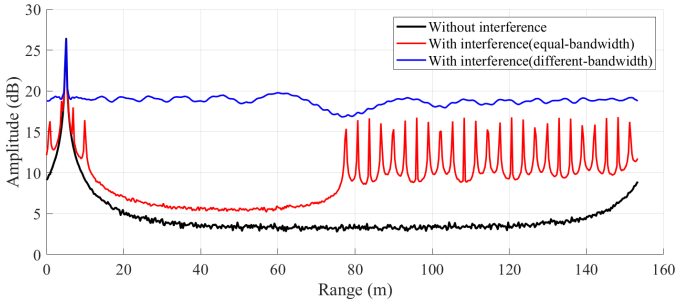

(b)

Fig. 3. Comparison of received signal characteristics under equal-bandwidth and different-bandwidth interference: (a) time-domain waveforms and (b) corresponding range profiles.

III. Proposed SF-IMNet for SF-FMCW Interference Mitigation

We propose SF-IMNet, a deep learning-based method to mitigate SF-FMCW interference in FMCW systems. The proposed method estimates the interference component contained in the received signal and mitigates its effect through interference subtraction. Fig. 4 illustrates the architecture of SF-IMNet. The network takes a complex-valued input consisting of the target-reflected FMCW signal, the SF-FMCW interference, and noise. It outputs an estimate of the interference component, which is used to obtain an interference-mitigated FMCW signal through subtraction from the received signal.

The input signal is represented as a two-channel array of size $(N_B \times 2 \times N \times P)$, where N_B denotes the batch size, N denotes the fast-time length, and P denotes the slow-time length. The encoder first expands the number of channels to 32 while maintaining the original spatial dimensions. After this expansion, the encoder applies three downsampling blocks that reduce the spatial dimension to $(N/8, P/8)$ and increase the channel dimension to 256. The reduced dimension enlarges the receptive field and allows the model to capture interference patterns that extend across multiple fast-time and slow-time regions. Each downsampling block first refines the features through two 3×3 convolution layers, followed by batch normalization and a rectified linear unit (ReLU) activation, and then applies max pooling to reduce the dimension.

To estimate the interference term from these high-level features, the decoder restores the spatial resolution through three upsampling blocks. Each block first increases the dimension by bilinear interpolation and then concatenates the corresponding encoder features through a skip connection. The block subsequently refines the combined features through two 3×3 convolution layers with batch normalization and ReLU activation. A final 1×1 convolution produces the estimated interference. To improve robustness to variations in interference patterns, data augmentation is applied during training. A horizontal flip is applied with a probability of 0.5 to prevent bias toward a specific interference slope orientation. The loss function consists of two terms: one measuring the accuracy of the predicted interference and the other evaluating the quality of the interference-mitigated signal. The total loss is defined as

$$\mathcal{L} = \frac{1}{2}\,\mathrm{MSE}\Big(\hat{\mathbf{I}}, \mathbf{I}\Big) + \mathrm{MSE}\Big(\hat{\mathbf{X}}, \mathbf{X}\Big)\,. \tag{7}$$

where $\hat{\mathbf{I}}$ denotes the predicted interference and $\hat{\mathbf{X}}$ denotes the interference-mitigated signal. The interference-mitigated signal is obtained as $\hat{\mathbf{X}} = \mathbf{Y} - \hat{\mathbf{I}}$, where $\mathbf{Y}$ denotes the received signal. The mean-square error for complex-valued data is defined as

$$\mathrm{MSE}(\mathbf{a}, \mathbf{b}) = \frac{1}{N_{\mathrm{B}} NP} \sum_{b,n,p} \Big(\big\| \Re\{a[b,n,p]\} - \Re\{b[b,n,p]\} \big\|^2 + \big\| \Im\{a[b,n,p]\} - \Im\{b[b,n,p]\} \big\|^2 \Big). \tag{8}$$

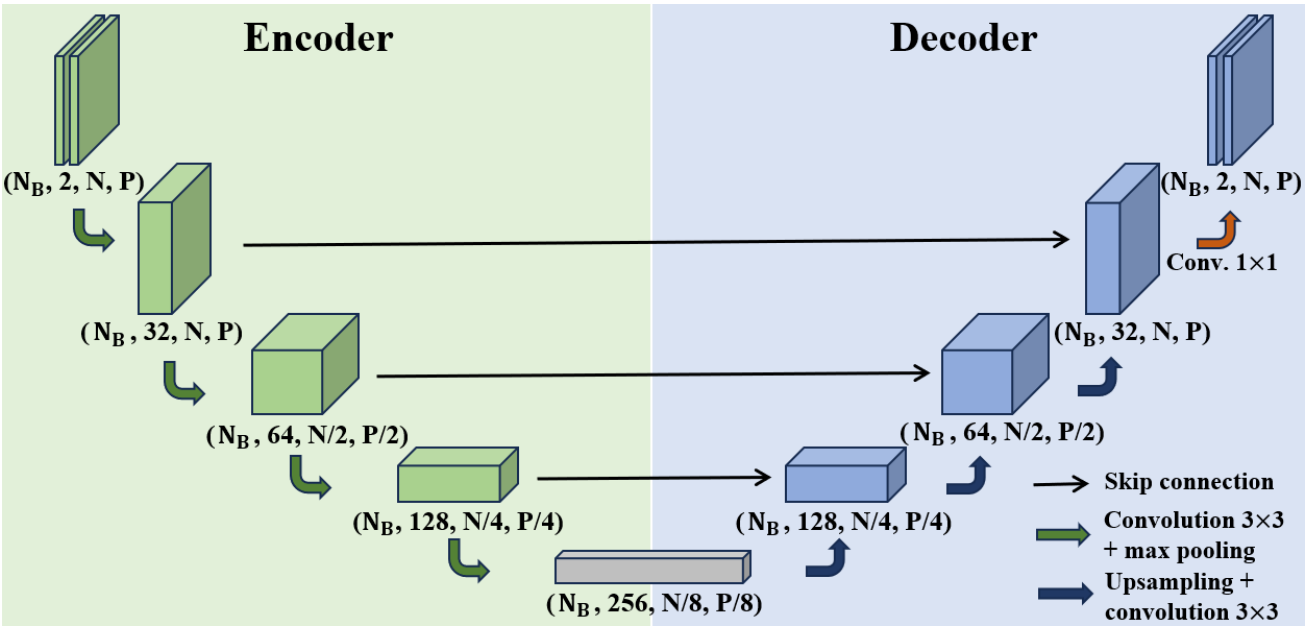

Fig. 4. Proposed U-Net-based SF-IMNet architecture for SF-FMCW interference mitigation. The encoder extracts large-scale interference patterns and the decoder restores spatial resolution while refining local structures.

and this formulation allows the network to learn both the real and imaginary parts of the interference and the interference-mitigated FMCW signal.

IV. Performance Evaluation

This section evaluates the interference mitigation performance of SF-IMNet. System parameters used in the simulation are listed in Table I. The interfering SF-FMCW system and the victim FMCW system employ the same carrier frequency and chirp duration. In each trial, the number of targets varies between 1 and 3, with their ranges and velocities uniformly distributed within $[0, 50]$ m and $[-50, 50]$ m/s. An SF-FMCW interferer is randomly positioned within a range of $[0, 50]$ m, with its velocity set between $[-50, 50]$ m/s. To reflect diverse interference configurations, the bandwidth of the interferer is set to either 100 or 500 MHz, and the frequency step size is chosen as either 1 or 2 MHz. In addition, AWGN is added with the SNR uniformly distributed between 10 and 30 dB.

The network is trained using the adaptive moment estimation optimizer for 100 epochs with a batch size of 32.

TABLE I
Simulation Parameters Used in the Performance Evaluation

Radar	Parameter	Value
Victim (FMCW)	Carrier frequency, f_c	77 GHz
	FMCW bandwidth, B_{F}	500 MHz
	Sampling frequency, f_s	50 MHz
	Fast-time samples, N	512
	Slow-time samples, P	128
	Chirp duration, T	20.48 μs
Interferer (SF-FMCW)	Carrier frequency, f_c'	77 GHz
	Interference bandwidth, B_{SF}	100 / 500 MHz
	Frequency step size, Δf	1 / 2 MHz
	Chirp duration, T	20.48 μs

The dataset consists of 10,000 simulated samples, which are partitioned into training, validation, and test sets in an 8:1:1 ratio. All reported results are obtained from the test set. The performance is evaluated using the signal-to-interference-plus-noise ratio (SINR) and correlation coefficient. The input SINR is computed as

$$\mathrm{SINR}_{\mathrm{in}} = 10\log_{10}\left(\frac{\|\mathbf{x}\|_2^2}{\|\mathbf{i}+\mathbf{n}\|_2^2}\right), \tag{9}$$

where $\mathbf{n}$ denotes AWGN. The output SINR measures how accurately the interference-mitigated signal matches the corresponding target-reflected FMCW signal and is defined as

$$\mathrm{SINR} = 10\log_{10}\left(\frac{\|\mathbf{x}\|_2^2}{\|\mathbf{x}-\hat{\mathbf{x}}\|_2^2}\right), \tag{10}$$

where $\hat{\mathbf{x}}$ denotes the interference-mitigated FMCW signal. The correlation coefficient is expressed as

$$\rho = \frac{\mathbf{x}^{\mathrm{H}}\hat{\mathbf{x}}}{\|\mathbf{x}\|_2\,\|\hat{\mathbf{x}}\|_2}, \tag{11}$$

where $|\rho|$ ranges from 0 to 1. Larger SINR values and correlation coefficients indicate superior mitigation of the SF-FMCW interference while ensuring a more accurate recovery of the desired target-reflected signal.

To show the effectiveness of SF-IMNet, we consider an example scenario with two targets located at ranges of 15 and 30 m and velocities of 5 and -3 m/s, respectively, together with an interfering SF-FMCW system located 20 m away and moving at -10 m/s. The signals before and after interference mitigation are examined in both the time domain and the range profile. In the equal-bandwidth configuration, the target-reflected signal contains strong periodic interference because

the receiving FMCW system and the SF-FMCW interferer operate with the same chirp bandwidth, as illustrated in Fig. 5 (a). After applying SF-IMNet, the interference-mitigated signal closely resembles the target-reflected FMCW signal, with the interference components substantially suppressed. The corresponding range profile is shown in Fig. 5 (b). Due to the SF-FMCW interference, the noise floor increases from 3.2 dB to 13.6 dB. After applying SF-IMNet, the noise floor is reduced to 3.8 dB, and the target-reflected components align with those of the interference-mitigated case. These results indicate that the proposed method effectively suppresses interference while preserving the target-reflected signal.

We also evaluate the different-bandwidth configuration under the same scenario. In this case, a short, high-amplitude spike appears in the time-domain signal because only a small portion of the SF-FMCW interference remains within the LPF passband, as shown in Fig. 6 (a). After applying SF-IMNet, the interference-mitigated signal closely resembles the interference-mitigated signal, indicating that the effect of the interference is effectively suppressed. The corresponding range profile is shown in Fig. 6 (b). The SF-FMCW interference elevates the noise floor across a wide range. After applying the proposed method, this noise floor elevation is significantly reduced, which confirms the effectiveness of SF-IMNet in suppressing different-bandwidth interference.

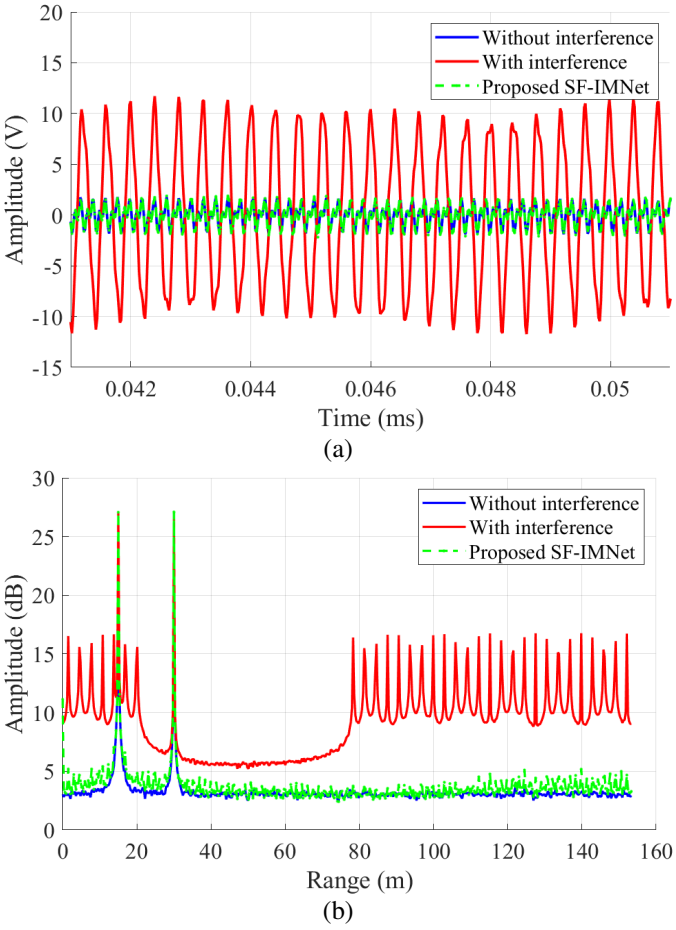

Fig. 5. Equal-bandwidth interference scenario: (a) time-domain waveforms without interference, with interference, and after applying the proposed SF-IMNet, and (b) corresponding range profiles.

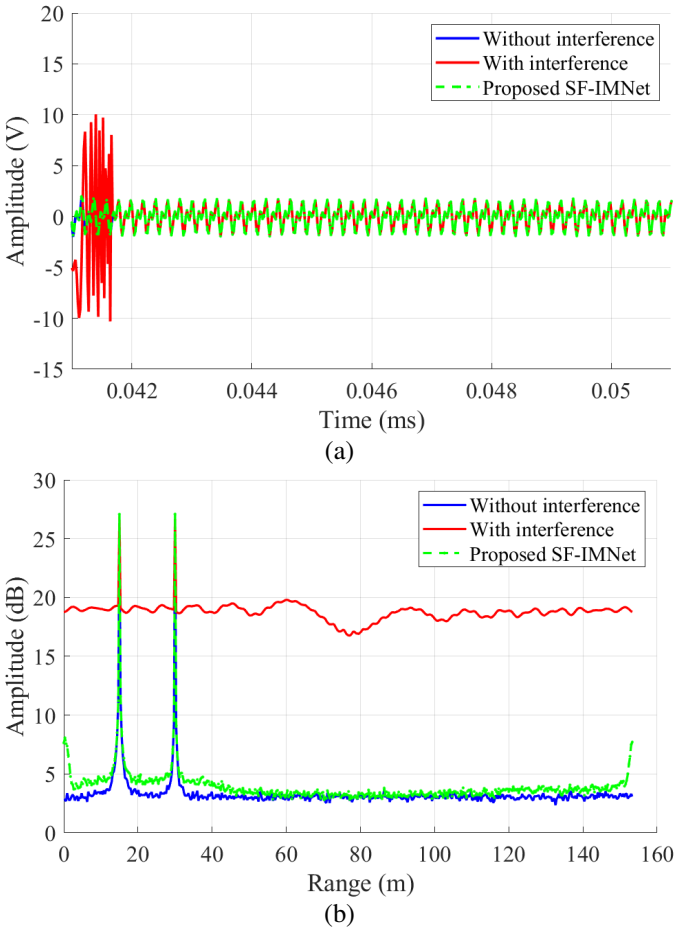

Fig. 6. Different-bandwidth interference scenario: (a) time-domain waveforms without interference, with interference, and after applying the proposed SF-IMNet, and (b) corresponding range profiles.

Next, we conduct a performance comparison with conventional interference mitigation methods: amplitude zeroing [12] and STFT interpolation [13]. Table II summarizes the evaluation results obtained from 100 Monte Carlo trials. The conventional methods exhibit limited performance, with output SINRs below 8 dB and correlation coefficients below 0.9. This degradation occurs because these conventional methods suppress the target-reflected signal along with the interference. In contrast, SF-IMNet consistently demonstrates superior interference mitigation performance across all tested scenarios, achieving an output SINR of 22.94 dB and a near-perfect

TABLE II
QUANTITATIVE COMPARISON OF INTERFERENCE MITIGATION METHODS

Method	**Output SINR (dB)**	$\lvert\rho\rvert$
Amplitude zeroing [12]	-1.16	0.693
STFT interpolation [13]	7.24	0.864
Proposed SF-IMNet	22.94	0.997

correlation coefficient of 0.997. This performance remains stable across a wide range of interference parameters, which suggests that the proposed method is robust to variations in the parameters of the interfering SF-FMCW system.

V. Conclusion

In this paper, we proposed SF-IMNet, a deep learning-based interference mitigation method for suppressing SF-FMCW interference in FMCW systems. The method estimates the two-dimensional interference component from the received signals and mitigates its effect through interference subtraction. Furthermore, SF-IMNet handled both equal-bandwidth and different-bandwidth interference scenarios and preserved the target-reflected FMCW signal across these cases. We verified the effectiveness of the proposed method through simulations that covered a wide range of target and interferer configurations. The method achieved an output SINR of 22.94 dB and a correlation coefficient of 0.997 at an input SINR of -10 dB. Moreover, compared with existing methods, the proposed SF-IMNet improved the SINR by up to 24.1 dB. These results demonstrated the strong interference mitigation capability of SF-IMNet under severe interference conditions and confirmed its stable performance across diverse scenarios.

Acknowledgment

This work was partly supported by Korea Institute for Advancement of Technology (KIAT) grant funded by the Korea Government (MOTIE) (P0020967, Advanced Training Program for Smart Sensor Engineers) and the National Research Foundation of Korea (NRF) grant funded by the Korea government (MSIT) (No. RS-2025-16068888).

References

[1] S. Campbell, N. O'Mahony, L. Krpalcova, D. Riordan, J. Walsh, and A. Murphy, "Sensor technology in autonomous vehicles: A review," *2018 29th Irish Signals and Systems Conference (ISSC)*, Belfast, UK, June 2018, pp. 1–6.

[2] E. Yurtsever, J. Lambert, A. Carballo, and K. Takeda, "A survey of autonomous driving: Common practices and emerging technologies," *IEEE Access*, vol. 8, pp. 58443–58469, March 2020.

[3] H. Park, C. Park, S. Kwak, and S. Lee, "MIMO FMCW radar-based indoor mapping through exploiting multipath signals," *IEEE Internet of Things Journal*, vol. 11, no. 19, pp. 31479–31491, October 2024.

[4] J. Hasch, E. Topak, R. Schnabel, T. Zwick, R. Weigel, and C. Waldschmidt, "Millimeter-wave technology for automotive radar sensors in the 77 GHz frequency band," *IEEE Transactions on Microwave Theory and Techniques*, vol. 60, no. 3, pp. 845–860, March 2012.

[5] J. Dickmann, J. Klappstein, M. Hahn, N. Appenrodt, H.-L. Bloecher, and K. Werber, "Automotive radar the key technology for autonomous driving: From detection and ranging to environmental understanding," *2016 IEEE Radar Conference (RadarConf)*, Philadelphia, PA, USA, May 2016, pp. 1–6.

[6] C. Waldschmidt, J. Hasch, and W. Menzel, "Automotive radar — From first efforts to future systems," *IEEE Journal of Microwaves*, vol. 1, no. 1, pp. 135–148, January 2021.

[7] S. Lee, J.-Y. Lee, and S.-C. Kim, "Mutual interference suppression using wavelet denoising in automotive FMCW radar systems," *IEEE Transactions on Intelligent Transportation Systems*, vol. 22, no. 2, pp. 887–897, February 2021.

[8] H. Lee, S.-Y. Kwon, and S. Lee, "Restoration of automotive radar signals under mutual interference by digital in-painting," *IEEE Transactions on Instrumentation and Measurement*, vol. 73, pp. 1–12, July 2024.

[9] M. Kahlert, T. Fei, C. Tebruegge, and M. Gardill, "An improved stepped-frequency PMCW waveform for automotive radar applications," *2024 15th German Microwave Conference (GeMiC)*, Duisburg, Germany, March 2024, pp. 193–196.

[10] Y. Gao, W. Wei, X. Yu, and G. Cui, "High-resolution detection of moving targets using stepped-frequency signal for mmWave FMCW radar," *2024 IEEE International Conference on Signal, Information and Data Processing (ICSIDP)*, Zhuhai, China, November 2024, pp. 1–6.

[11] Y. Li, W. Xia, L. Zhu, C. Qu, X. Rui, and J. Zhou, "Distributed MIMO radar network for IoT: high-resolution 4-D point cloud generation and signal processing for smart mobility," *IEEE Internet of Things Journal*, vol. 12, no. 12, pp. 22366–22380, June 2025.

[12] J.-H. Choi, H.-B. Lee, J.-W. Choi, and S.-C. Kim, "Mutual interference suppression using clipping and weighted-envelope normalization for automotive FMCW radar systems," *IEICE Transactions on Communications*, vol. E99.B, no. 1, pp. 280–287, January 2016.

[13] S. Neemat, O. Krasnov, and A. Yarovoy, "An interference mitigation technique for FMCW radar using beat-frequencies interpolation in the STFT domain," *IEEE Transactions on Microwave Theory and Techniques*, vol. 67, no. 3, pp. 1207–1220, March 2019.